An Online Global Fault-Tolerant Control Strategy for Symmetrical Multiphase Machines With Minimum Losses in Full Torque Production Range

Jiawei Sun, *Student Member, IEEE*, Zicheng Liu, *Member, IEEE*, Zedong Zheng, *Senior Member, IEEE*, and Yongdong Li, *Member, IEEE*

***Abstract*—The high fault-tolerant ability of multiphase drives is favored in safety-critical applications. Under open-phase faults, to guarantee ripple-free torque, stator current references should be revised. In this paper, a global fault-tolerant control strategy based on an online current optimization algorithm (OCOA) is proposed for symmetrical multiphase machines (SMMs) to achieve both the maximal torque production range (TPR) and minimal stator winding losses under all possible OPFs. The OCOA can calculate the minimum losses current references covering the full TPR online, regardless of the number and locations of faulty phases. With the online-optimized references, ripple-free torque and minimum losses in full TPR can be achieved under faulty conditions. Additionally, the proposed method can be adopted to SMMs with arbitrary phase numbers. Simulation and experiments demonstrate that the online optimization can be completed in a short time, meanwhile, achieves the same TPR and loss reduction compared with an existing offline strategy based on prestored look-up tables. Due to the flexible online calculation ability and excellent extensibility, the proposed method is especially favored in modular multiphase converters and machines with high phase numbers, where converters can adapt to machines with different phase numbers or the number of possible faulty conditions can be extremely large.**

***Index Terms*—Fault tolerance, induction motor drives, multiphase drives, optimal current control, variable speed drives.**

I. Introduction

MULTIPHASE drive systems have been an interesting subject in recent years due to its high reliability [1], high power density [2], and especially the ability to achieve the fault-tolerant control by exploiting additional degrees of control freedom [3]. The high fault-tolerant ability of multiphase machines is suitable for safety-critical applications (e.g., electric ship propulsion) and is also a hot topic in the existing literature [4], [5].

Different types of faults in multiphase drive systems were discussed in [6] and [7] and most of the faults can be converted into open-phase faults (OPFs) by some suitable ways (e.g., additional protection devices) [8], [9]. Therefore, most research efforts are focused on fault-tolerant control against OPFs [10], [11].

Fault-tolerant control methods for multiphase machines can be mainly divided into three categories. The first category tries to reconstruct the decoupled machine model under different faulty conditions [12], [13]. However, the process to obtain the decoupled model and transform matrix is complicated and depends on the position and number of faulty phases [14]; therefore, this approach is not widely used even though fully decoupled fault-tolerant operation can be achieved [15]. The second category focuses on improving the robustness of the algorithm without altering the control method, such as the robust fault-tolerant control [16], [17], but the algorithm is complex and the computational cost is relatively high. More importantly, the precise control of currents in the torque-producing subspace, α_1-β_1, cannot be achieved and considerable torque ripples are still induced under faulty conditions. The last category focuses on the optimal current control using PR controllers or anti-synchronous PI controllers with current references obtained in offline optimization [8], [18]. This strategy has been widely studied by researchers because of the advantages of easier implementation, potential for adapting to various faulty conditions, and robust fault-tolerant performance.

The strategy for calculating the post-fault phase current references is important and has a great influence on the performance of optimal current control. Two common strategies for determining these current references have been proposed: maximum torque (MT) and minimum losses (ML) [8], [18]. The MT strategy aims at the widest current amplitude range in torque-producing plane while ensuring that all the phase current amplitudes are below the rated value [19]. This typically leads to equal phase current amplitudes and the widest torque production range (TPR). Still, there are a few exceptions where the phase current amplitudes are not equal under MT strategy. The ML strategy aims to minimize the stator winding losses, leading to unequal phase current amplitudes, and more efficient operation [20]. The MT and ML strategies were studied and

Manuscript received January 25, 2019; revised April 25, 2019 and June 16, 2019; accepted June 23, 2019. Date of publication July 8, 2019; date of current version December 13, 2019. Recommended for publication by Associate Editor S. S. Krishnamoorthy. *(Corresponding author: Zedong Zheng.)*

J. Sun, Z. Zheng, and Y. Li are with the State Key Laboratory of Power System, Department of Electrical Engineering, Tsinghua University, Beijing 100084, China (e-mail: thu_sjw@126.com; zzd@ tsinghua.edu.cn; liyd@mail.tsinghua.edu.cn).

Z. Liu is with the School of Electrical and Electronic Engineering, Huazhong University of Science and Technology, Wuhan 430074, China (e-mail: liuzc_thu@163.com).

Color versions of one or more of the figures in this paper are available online at http://ieeexplore.ieee.org.

Digital Object Identifier 10.1109/TPEL.2019.2927382

TABLE I
NUMBER OF DIFERENT OPF CONDITIONS IN A SYMMETRICAL NINE-PHASE MACHINE WITH ONE NEUTRAL POINT

Number of faulty phases	Number of faulty conditions
1	1
2	4
3	10
4	14
5	14
6	10
Total	53

compared for various kinds of multiphase machines in [9], [18], and [21].

Typically, optimal current references for the MT and ML strategies are calculated offline. However, the offline method has two main limitations. First, the offline method lacks generality and extensibility. The offline calculated references can only be used in the fault-tolerant control of machines with the specific phase number and neutral point connection. If a machine with a different phase number or neutral point connection is used, all the references need to be reoptimized and stored in the controller, which is inconvenient and time-consuming. Second, it is difficult to implement global ML fault-tolerant control on a machine with a large phase number because the optimal references depends on the phase number, the number of faulty phases and their locations, and the load level [9], hence numerous optimal references have to be calculated offline and stored in the controller. In the MT and ML strategy, only one group of references need to be optimized and stored for one possible faulty condition, thus the total computational efforts and storage cost is small. However, neither MT nor ML strategy can achieve minimal stator losses in full TPR. The MT strategy can operate over full TPR but the losses are high, while the ML strategy has the minimized losses for a given torque at the expense of a reduction of the TPR [22]. In [9], the concept of the unified global fault-tolerant optimal current control was proposed, which can achieve ML and smooth torque production in open-phase and short-circuit faults. However, this method requires the storage of the constraint matrices, which will occupy considerable storage space if the machine phase number is high. Also, the method in [9] failed to include the constraint of maximal phase rms current, which causes a reduced TPR compared to the MT strategy. In [22], control strategy for minimal losses operation in full TPR under the single OPF was proposed, but offline optimizations and phase current references look-up tables were used, thus it is difficult to apply this strategy to machines with a large number of phases because the number of possible OPF conditions rises dramatically with the phase number. Take the nine-phase symmetrical multiphase machine (SMMs) with one neutral point, for example, and the possible numbers of OPF conditions with consideration of the rotational symmetry are listed in Table I. If offline optimization method is used for global fault-tolerant control for the nine-phase machine, 53 look-up tables need to be calculated offline and stored in the controller, which requires considerable calculation efforts and storage cost. For machines with more phases, such as the 15-phase machines, it will even be more difficult to apply the offline method because more than one thousand OPF conditions may exist.

This paper presents an online fault-tolerant control strategy with minimal losses in full TPR) based on a simple online current optimization algorithm (OCOA), which can be applied to SMMs with an arbitrary number of phases. Phase current references with minimal losses covering the full TPR is calculated online according to the present faulty condition. When machine torque is within the TPR of ML operation, the phase current references are the same as the ML strategy, thus ML operation is achieved. When machine torque is beyond the TPR of ML operation, the optimized phase current references can provide the given torque reference without causing overcurrent in any phase, while losses are also minimized. As load torque reaches the upper bound of the TPR in MT operation, optimized references finally converge to the MT phase current references. Therefore, both full TPR and minimal losses can be guaranteed. The online optimization algorithm was evaluated for machines with different phase numbers and experimental results were demonstrated on a nine-phase induction machine (IM). Experimental results show that the proposed method is simple enough to be implemented online. Compared with the FRML strategy proposed in [22], the same TPR and loss reduction can be achieved without offline optimizations and prestored look-up tables. When the OCOA is applied to machines with different phase numbers and neutral point connections, only few parameters need to be adjusted, which is much more convenient and time-saving than the FRML strategy. The generality and extensibility of the proposed method are especially suitable for use in fault-tolerant modular multiphase converters. By combining this online strategy with the modular multiphase converters, the converter system can easily achieve fault-tolerant operation for machines with different phase numbers in different drives and applications, which avoids the repeated current references calculating and storing process. Also, the proposed method is especially suitable for the global optimal fault-tolerant control of machines with large phase numbers due to the avoidance of calculating and storing large-scale look-up tables.

This paper is organized as follows. The general model of SMMs is given in Section II. The online optimization algorithm is described in Section III. The experimental setup and results are presented in Section IV. Section V concludes this paper.

II. GENERAL MODEL OF SMMS

In this section, the definition of SMMs discussed in this paper is clarified and a general machine model is derived. A multiphase machine is called an SMM if and only if the stator-winding configuration has rotational symmetry of order *m*, where *m* is the phase number. In other words, if the stator-winding configuration is rotated by an angle of $\alpha = 2\pi/m$, the derived stator-winding configuration is equivalent to the original one. An example is given in Fig. 1, where two possible stator-winding configurations for nine-phase SMMs are demonstrated. Noticing that the windings with different color have different neutral points.

SMMs can be modeled into several subspaces, among which are $m - 2n_s$ subspaces correspond to $m - 2n_s$ zero-sequence

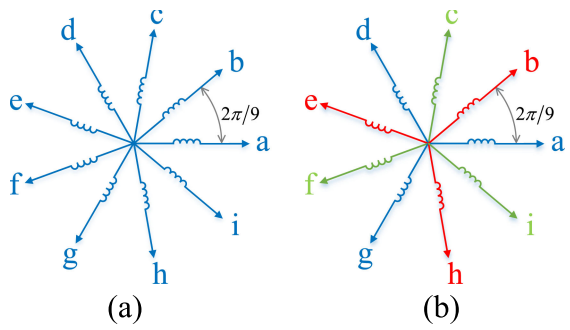

Fig. 1. Two possible stator-winding configurations for nine-phase SMMs (windings with different color have different neutral points). (a) Single-neutral-point configuration. (b) Three-neutral-point configuration.

axes. The other n_s subspaces are denoted by α_1-β_1, $\alpha_{s_2}-\beta_{s_2}$, $\alpha_{s_3}-\beta_{s_3}$, …, $\alpha_{s_{n_s}}-\beta_{s_{n_s}}$, where $n_s = \text{floor}((m-n_{\text{np}})/2)$ [2]. Floor(x) maps x to the largest integer which is not greater than x. n_{np} is the number of neutral points. If $m-n_{\text{np}}$ is an even number, $m-2n_s = n_{\text{np}}$ and each zero-sequence axis corresponds to the zero-sequence component of a group of windings sharing the same neutral point. Otherwise, $m-2n_s = n_{\text{np}}+1$ and an extra zero-sequence axis should be designed [2]. As only odd order space harmonics exist, the commonly used subspaces are $\alpha_s-\beta_s$ where s is an odd number and $s \neq k(m/n_{\text{np}})$, $k = 1, 2, 3, \ldots$. The phase variables vector $\boldsymbol{v}_p$ can be transformed into these subspaces and zero-sequence axes if multiplied by a transformation matrix $\boldsymbol{T}$ as shown in (2), where $\boldsymbol{v}_{\alpha\beta 0}$ is a vector of variables after the transformation. The operator ^{T} denotes the transpose operation of a matrix [22]

$$\boldsymbol{v}_{\alpha\beta 0} = \boldsymbol{T}\boldsymbol{v}_p \tag{1}$$

$$\boldsymbol{T} = \sqrt{\frac{2}{m}}\left[\boldsymbol{T}_1\ \boldsymbol{T}_{s_2}\ \cdots\ \boldsymbol{T}_{s_{n_s}}\ \boldsymbol{z}_1\ \boldsymbol{z}_2\ \cdots\ \boldsymbol{z}_{m-2n_s}\right]^T \tag{2}$$

where

$$\boldsymbol{T}_n = \begin{bmatrix} 1 & \cos(n\alpha) & \cos(2n\alpha) & \cdots & \cos((m-1)n\alpha) \\ 0 & \sin(n\alpha) & \sin(2n\alpha) & \cdots & \sin((m-1)n\alpha) \end{bmatrix}^T \tag{3}$$

corresponds to the $\alpha_n-\beta_n$ subspace. And $\boldsymbol{z}_1, \boldsymbol{z}_2, \ldots, \boldsymbol{z}_{m-2n_s}$, whose elements are determined by the configuration of neutral points, correspond to the zero-sequence axes.

Components $v_{\alpha 1}$ and $v_{\beta 1}$ in α_1–β_1 subspace can be projected onto a synchronous reference frame d_1–q_1, where the d_1 axis is aligned with the rotor flux, which is generated by the magnetizing currents in an IM or by permanent magnets in a permanent magnet synchronous machine [2].

For an IM with sinusoidally distributed windings, the model in d_1-q_1 frame can be expressed as [16]

$$\begin{bmatrix} u_{sd1} \\ u_{sq1} \end{bmatrix} = \begin{bmatrix} R_s & -\omega L_{lk} \\ \omega L_{lk} & R_s \end{bmatrix}\begin{bmatrix} i_{sd1} \\ i_{sq1} \end{bmatrix} + L_{lk}\frac{d}{dt}\begin{bmatrix} i_{sd1} \\ i_{sq1} \end{bmatrix} + \frac{L_{m1}}{L_{r1}}\begin{bmatrix} \frac{d}{dt} \\ \omega_s \end{bmatrix}\psi_{rd1} \tag{4}$$

$$\frac{d\psi_{rd1}}{dt} = \frac{L_{m1}i_{sd1}-\psi_{rd1}}{\tau_{r1}} \tag{5}$$

$$\omega = \omega_r + \frac{L_{m1}}{\tau_{r1}}\frac{i_{sq1}}{\psi_{rd1}} \tag{6}$$

$$T_e = p\frac{L_{m1}}{L_{r1}}i_{sq1}\psi_{rd1} \tag{7}$$

where u and i stand for voltage and current, respectively; R_s and L_{lk} are the stator resistance and stator leakage inductance, $L_{lk} = L_{s1} - L_{m1}^2/L_{r1}$; L_{s1}, L_{m1}, and L_{r1} are the stator inductance, mutual inductance between stator and rotor, and rotor inductance; ψ_{rd1} is the rotor flux; τ_{r1} is the rotor time constant; ω is the synchronous electric angular speed; ω_r is the rotor electric angular speed; T_e is the electromagnetic torque and p is the number of pole pairs.

For a PMSM, the model in d_1-q_1 is expressed as [23]

$$\begin{bmatrix} u_{sd1} \\ u_{sq1} \end{bmatrix} = \begin{bmatrix} R_s & -\omega L_{q1} \\ \omega L_{d1} & R_s \end{bmatrix}\begin{bmatrix} i_{sd1} \\ i_{sq1} \end{bmatrix} + \begin{bmatrix} L_{d1} \\ L_{q1} \end{bmatrix}^T \frac{d}{dt}\begin{bmatrix} i_{sd1} \\ i_{sq1} \end{bmatrix} + \omega\begin{bmatrix} 0 \\ \psi_r \end{bmatrix} \tag{8}$$

$$T_e = p\left(\psi_r i_{q1} + (L_{d1}-L_{q1})\, i_{d1} i_{q1}\right) \tag{9}$$

where L_{d1} and L_{q1} are the stator inductances in d_1 axis and q_1 axis, respectively; ψ_r is the rotor flux.

The model in other subspaces are the same for IM and PMSM, which can be expressed as [23]

$$\begin{bmatrix} u_{\alpha(s)} \\ u_{\beta(s)} \end{bmatrix} = R_s\begin{bmatrix} i_{\alpha(s)} \\ i_{\beta(s)} \end{bmatrix} + L_{lk}\frac{d}{dt}\begin{bmatrix} i_{\alpha(s)} \\ i_{\beta(s)} \end{bmatrix} \tag{10}$$

where $s \neq 1$.

From (7) and (9), a smooth torque and stator flux can be achieved if the trajectory of the current space vector in α_1–β_1 is a circle, no matter the machine is in a healthy or faulty situation [18].

III. Online Current Optimization Algorithm

In this section, the OCOA is presented for SMMs. First, the ML redistribution (MLR) is introduced for calculating the ML phase current references. Second, the algorithm for calculating the optimized phase current references when machine torque is beyond the TPR of the ML strategy is demonstrated. The OCOA is evaluated on SMMs with different phase numbers and winding configurations via simulation.

A. Online Calculation of ML Phase Current References

Referring to [18] and [22], for an SMM with sinusoidally distributed windings, not considering the constraint on maximal phase rms current and normalize the current with $\sqrt{(2/m)}\, I_{\alpha\beta 1}$, where $I_{\alpha\beta 1}$ is the amplitude of the current space vector in α_1–β_1, the ML optimization problem can be described as

$$\min\left(\boldsymbol{I}^T\boldsymbol{I}\right) \tag{11}$$

subject to

$$\begin{aligned} \boldsymbol{CI} &= [\boldsymbol{b} \quad \boldsymbol{0}]^T \\ \boldsymbol{FI} &= \boldsymbol{0} \end{aligned} \tag{12}$$

where

$$\boldsymbol{I} = \begin{bmatrix} i_1 & i_2 & \cdots & i_m \end{bmatrix}^T \tag{13}$$

$$\boldsymbol{C} = \begin{bmatrix} \boldsymbol{T}_1{}^T & \boldsymbol{Z}^T \end{bmatrix}^T \tag{14}$$

$$\boldsymbol{b} = (m/2) \cdot \begin{bmatrix} \cos\omega t & \sin\omega t \end{bmatrix}^T. \tag{15}$$

$\boldsymbol{I}$ is the vector of phase current references. i_k is the reference for phase k current. $\boldsymbol{C}$ is the constraint matrix containing the current space vector trajectory constraint and the zero-sequence current constraint. t is the time variable. $\boldsymbol{Z}$ is the zero-sequence current constraint matrix given in (16), where $\boldsymbol{I}_{n_{np}\times n_{np}}$ is the identity matrix with n_{np} rows and n_{np} columns [22]

$$\boldsymbol{Z} = \begin{bmatrix} \boldsymbol{I}_{n_{\mathrm{np}}\times n_{\mathrm{np}}} & \boldsymbol{I}_{n_{\mathrm{np}}\times n_{\mathrm{np}}} & \cdots & \boldsymbol{I}_{n_{\mathrm{np}}\times n_{\mathrm{np}}} \end{bmatrix}. \tag{16}$$

$\boldsymbol{F}$ is the OPF constraint matrix. Assuming n_f phases are open-phase and they are phase f_1, phase f_2, …, and phase f_{n_f}, the corresponding OPF is denoted by OPF $(f_1, f_2, \ldots, f_{n_f})$.$\boldsymbol{F}_{\mathrm{OPF}(f_1,f_2,\ldots,f_{n_f})}$ is the fault constraint matrix under OPF $(f_1, f_2, \ldots, f_{n_f})$ and only the elements shown in (17) are nonzero in the fault constraint matrix.$\boldsymbol{F}_{\mathrm{OPF}(f_1,f_2,\ldots,f_{n_f})}(n, f_n)$ is the element in the nth row and f_nth column of $\boldsymbol{F}_{\mathrm{OPF}(f_1,f_2,\ldots,f_{n_f})}$ [9]

$$\boldsymbol{F}_{\mathrm{OPF}\left(f_1,f_2,\ldots,f_{n_f}\right)}(n, f_n) = 1, \quad n = 1, 2, \ldots, n_f. \tag{17}$$

If the machine is in a healthy situation, the optimal reference is

$$\boldsymbol{I}_h = \begin{bmatrix} i_{1\_h} & i_{2\_h} & \cdots & i_{m\_h} \end{bmatrix}^T. \tag{18}$$

If the first phase is open and the current references in other phases remain the same as (18), referring to (3), (12), and (14), we have

$$\boldsymbol{T}_1 \begin{bmatrix} 0 & i_{2\_h} & i_{3\_h} & \cdots & i_{m\_h} \end{bmatrix}^T = \boldsymbol{b} - i_{1\_h} \begin{bmatrix} 1 & 0 \end{bmatrix}^T = \boldsymbol{b}'. \tag{19}$$

Apparently, the trajectory of $\boldsymbol{b}$'is not a circle. To keep the circular trajectory of current vector, the current references in healthy phases should be revised to compensate the lost i_{1_h}, the compensation current reference in phase k is denoted as i_{k_c} and these references must satisfy

$$\boldsymbol{T}_1 \begin{bmatrix} 0 & i_{2\_c} & i_{3\_c} & \cdots & i_{m\_c} \end{bmatrix} = i_{1\_h} \begin{bmatrix} 1 & 0 \end{bmatrix}^T. \tag{20}$$

We set i_{k_c} has the form of (21), where r_k is a constant

$$i_{k\_c} = r_k i_{1\_h}. \tag{21}$$

Substitute (21) into (20) we have

$$\boldsymbol{T}_1 \begin{bmatrix} 0 & r_2 & r_3 & \cdots & r_m \end{bmatrix} = \begin{bmatrix} 1 & 0 \end{bmatrix}^T \tag{22}$$

which is a set of undetermined linear equations, thus r_k has infinite solutions. However, we are only interested in the ML current references. In this case, r_k can be uniquely determined as

$$r_{k\_\mathrm{ML}} = \left(i_{k\_\mathrm{ML\_OPF(1)}} - i_{k\_h}\right) / i_{1\_h} \tag{23}$$

where r_{k_ML} is the coefficient corresponding to the ML references under OPF(1) and $i_{k\_ML\_OPF(1)}$ is the ML current reference in phase k under OPF(1). The current reference after the compensation is

$$\begin{aligned} \boldsymbol{I}_{\mathrm{ML\_OPF(1)}} &= \boldsymbol{I}_h + i_{1\_h} \begin{bmatrix} -1 & r_{2\_\mathrm{ML}} & r_{3\_\mathrm{ML}} & \cdots & r_{m\_\mathrm{ML}} \end{bmatrix} \\ &= \begin{bmatrix} 0 & i_{2\_\mathrm{ML\_OPF(1)}} & i_{3\_\mathrm{ML\_OPF(1)}} & \cdots & i_{m\_\mathrm{ML\_OPF(1)}} \end{bmatrix}. \end{aligned} \tag{24}$$

Under OPF(1), the ML references changes from $\boldsymbol{I}_h$ to $\boldsymbol{I}_{ML\_OPF(1)}$ as shown in (24). This alternation can be intuitively regarded as a redistribution of the current reference in the faulty phase to other healthy phases. We can further derive the expression for the redistribution of current reference in any phase k as

$$\boldsymbol{I}_{\mathrm{MLR}(k)} = \boldsymbol{I}_0 + i_{k\_0} \boldsymbol{R}_{\mathrm{MLR}(k)} \tag{25}$$

where $\boldsymbol{I}_{\mathrm{MLR}(k)}$ is the current reference vector after the redistribution, $\boldsymbol{I}_0$ is the original current reference vector, i_{k_0} is the kth element of $\boldsymbol{I}_0$ and $\boldsymbol{R}_{\mathrm{MLR}(k)}$ is the redistribution vector given in (26), where $\boldsymbol{R}_{\mathrm{MLR}(k)}(n)$ is the nth element in $\boldsymbol{R}_{\mathrm{MLR}(k)}$

$$\boldsymbol{R}_{\mathrm{MLR}(k)}(n) = \begin{cases} r_{(m-k+n+1)\_\mathrm{ML}}, & 0 < n < k \\ -1, & n = k \\ r_{(n-k+1)\_\mathrm{ML}}, & k < n < m. \end{cases} \tag{26}$$

In this paper, the current reference vector is recorded as

$$\begin{aligned} \boldsymbol{I} &= \cos\omega t \cdot \boldsymbol{x} + \sin\omega t \cdot \boldsymbol{y} \\ \boldsymbol{x} &= \begin{bmatrix} x_1 & x_2 & \cdots & x_m \end{bmatrix}^T \\ \boldsymbol{y} &= \begin{bmatrix} y_1 & y_2 & \cdots & y_m \end{bmatrix}^T \end{aligned} \tag{27}$$

where $\boldsymbol{x}$ and $\boldsymbol{y}$ are cosine and sine components reference vector, respectively. Therefore, (25) can be rewritten as

$$\begin{aligned} \boldsymbol{x}_{\mathrm{MLR}(k)} &= \boldsymbol{x}_0 + x_{k\_0} \boldsymbol{R}_{\mathrm{MLR}(k)} \\ \boldsymbol{y}_{\mathrm{MLR}(k)} &= \boldsymbol{y}_0 + y_{k\_0} \boldsymbol{R}_{\mathrm{MLR}(k)}. \end{aligned} \tag{28}$$

The aforementioned equation is called the ML redistribution of phase k current reference (abbreviated as MLR(k)) in this paper. The MLR operation has one important property is that in (25), if

$$\boldsymbol{CI}_0 = \boldsymbol{0} \tag{29}$$

then

$$\boldsymbol{CI}_{MLR(k)} = \boldsymbol{0}. \tag{30}$$

The current trajectory constraint and zero-sequence current constraint are automatically preserved after MLR operations.

Due to the rotational symmetry of SMMs, ML references under OPF(k) can be obtained by performing one MLR(k) operation on $\boldsymbol{I}_{\mathrm{h}}$. When multiple phases are in faulty condition, an intuitive method for calculating the ML current references is to redistribute all the current references in faulty phases to healthy phases with MLR operations. One problem is that after redistribution of current reference in one faulty phase, current references in other faulty phases will also be changed and may not equal to zero. Therefore, the MLR operations must be carried

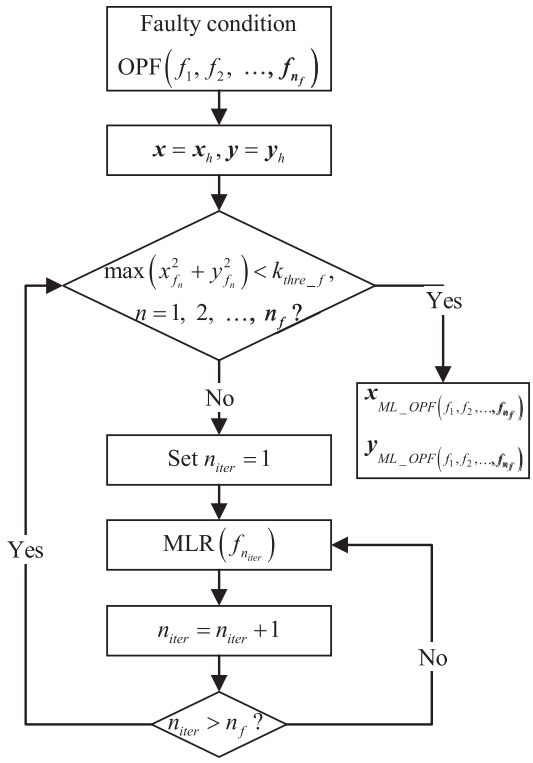

Fig. 2. Algorithm for online calculation of ML current references.

out iteratively. The block diagram for ML optimization is given in Fig. 2.

As shown in Fig. 2, once the faulty phases are determined, the current references are initialized with $\boldsymbol{x}_h$ and $\boldsymbol{y}_h$, which are the optimal cosine and sine reference vectors under the healthy condition. Then the algorithm checks if the maximal amplitude of current references in faulty phases exceeds the small threshold value $k_{\mathrm{thre\_}f}$. If so, the maximal reference in faulty phases is eliminated and redistributed with MLR to other phases. By doing the MLR operations continuously, because the redistribution coefficient r_{k_ML} is less than 1, the remaining current references in faulty phases will keep decreasing. Finally, these references are all below $k_{\mathrm{thre\_}f}$ and the faulty condition constraint is satisfied. Considering the property of MLR given in (29) and (30), the current trajectory constraint and the zero-sequence current constraint are also satisfied. Therefore, all the constraints are satisfied and the final calculated current reference vector will be the ML reference vector under the given faulty condition. To validate the optimality of the final solutions, numerical simulations are done for various SMMs. During the optimization, the error between the calculated references and the optimized references can be described as (31) shown at the bottom of this page, where $\boldsymbol{x}_{\mathrm{cal}}$ and $\boldsymbol{y}_{\mathrm{cal}}$ are the vector of calculated current references during the online optimization process. The two vectors $\boldsymbol{x}_{\mathrm{ML\_OPF}(f_1,\ldots,f_{n_f})}$ and $\boldsymbol{y}_{\mathrm{ML\_OPF}(f_1,\ldots,f_{n_f})}$ are the optimal current references. $|\boldsymbol{x}|$ is the Euclidean norm of vector $\boldsymbol{x}$. The relationship between d_{norm} and the number of MLR operations during the simulation is given in Fig. 3.

In Fig. 3, the ML optimization algorithm was evaluated on four different SMMs. For each machine, six different faulty conditions are demonstrated. The calculated references converge to the optimal values within 20 iterations. The optimization algorithm is suitable for online implementation because each MLR needs only $2(m-1)$ multiplications and $2(m-1)$ additions, which is not a big burden for available microcontrollers.

The optimized ML phase current references need to be further processed according to the type of current controller. For example, in this paper, the current controller proposed in [24] is integrated with the harmonic suppression control to achieve both fault-tolerant current control and reduced current harmonics. The schematic of the current controller is given in Fig. 4. In this control scheme, the fundamental phase current references need to be transformed into positive and negative sequence references. The equations for the transformation are given in (32). The positive and negative sequence references are fed into the current controllers on the fundamental plane to regulate the fundamental currents.

The current references for the harmonic plane are all set to zero to suppress the harmonic currents. Only the kth order positive sequence current harmonic in subspace $\alpha_k - \beta_k$ is compensated because it typically has the largest amplitude in the healthy condition and the computational resources are

$$\begin{bmatrix} i_{d_{(s)}+} \\ i_{q_{(s)}+} \\ i_{d_{(s)}-} \\ i_{q_{(s)}-} \end{bmatrix} = \begin{bmatrix} k_{d_{(s)}+} & l_{d_{(s)}+} \\ k_{q_{(s)}+} & l_{q_{(s)}+} \\ k_{d_{(s)}-} & l_{d_{(s)}-} \\ k_{q_{(s)}-} & l_{q_{(s)}-} \end{bmatrix} \begin{bmatrix} i_{d1+} \\ i_{q1+} \end{bmatrix}$$

$$k_{d_{(s)}+} = \frac{a_s + d_s}{m},\ k_{q_{(s)}+} = \frac{c_s - b_s}{m},\ l_{d_{(s)}+} = -k_{q_{(s)}+},$$

$$l_{q_{(s)}+} = k_{d_{(s)}+} k_{d_{(s)}-} = \frac{a_s - d_s}{m},$$

$$k_{q_{(s)}-} = \frac{b_s + c_s}{m},\ l_{d_{(s)}-} = k_{q_{(s)}-}, l_{q_{(s)}-} = -k_{d_{(s)}-}$$

$$a_s = \sum_{k=1}^{m} x_k \cos\left(s\left(k-1\right)\alpha\right)$$

$$b_s = \sum_{k=1}^{m} y_k \cos\left(s\left(k-1\right)\alpha\right)$$

$$c_s = \sum_{k=1}^{m} x_k \sin\left(s\left(k-1\right)\alpha\right)$$

$$d_s = \sum_{k=1}^{m} y_k \sin\left(s\left(k-1\right)\alpha\right) \tag{32}$$

$$d_{\mathrm{norm}} = \left(\frac{\left| \left[\boldsymbol{x}_{\mathrm{cal}}{}^T \ \boldsymbol{y}_{\mathrm{cal}}{}^T \right]^T - \left[\boldsymbol{x}_{\mathrm{ML\_OPF}\left(f_1,\ldots,f_{n_f}\right)}{}^T \ \boldsymbol{y}_{\mathrm{ML\_OPF}\left(f_1,\ldots,f_{n_f}\right)}{}^T \right]^T \right|}{\left| \left[\boldsymbol{x}_h{}^T \ \boldsymbol{y}_h{}^T \right]^T - \left[\boldsymbol{x}_{\mathrm{ML\_OPF}\left(f_1,\ldots,f_{n_f}\right)}{}^T \ \boldsymbol{y}_{\mathrm{ML\_OPF}\left(f_1,\ldots,f_{n_f}\right)}{}^T \right]^T \right|} \right)^2 \tag{31}$$

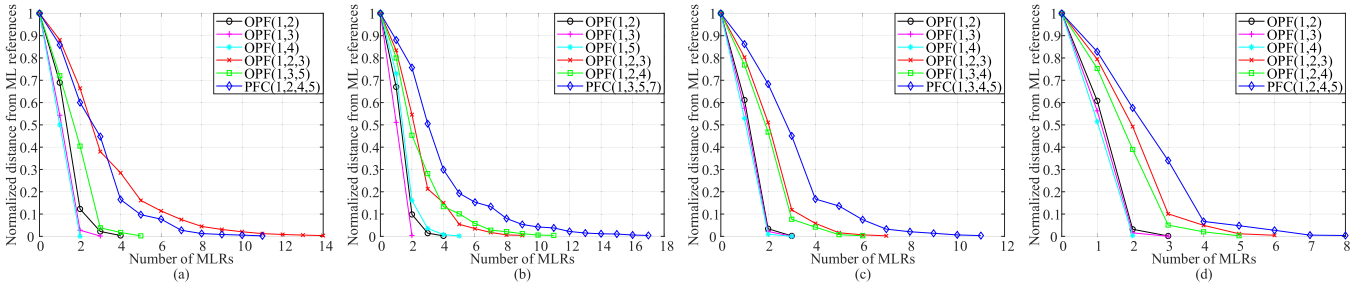

Fig. 3. Convergence process of the calculated current references to the ML current references. (a) Nine-phase SMM with one neutral point. (b) Nine-phase SMM with three neutral points. (c) Fifteen-phase SMM with one neutral point. (d) Fifteen-phase SMM with five neutral points.

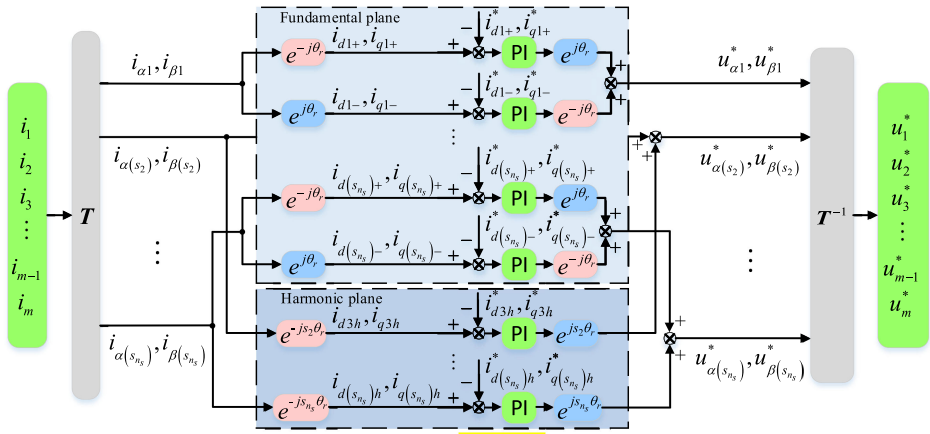

Fig. 4. Current control scheme with fundamental current regulation and harmonic suppression.

limited [25]. Noticing that in faulty conditions, large current harmonics may be induced in all the machine subspaces and both positive sequence and negative sequence can exist. In healthy condition, the most significant positive sequence current harmonics are compensated, thus phase currents with the relatively small distortion can be guaranteed. However, the severe asymmetry caused by faults will enlarge negative sequence harmonic currents and harmonic currents in other subspaces. Therefore, much more distorted currents are expected to be observed under fault-tolerant operation. In the meanwhile, current harmonics in the rotor and corresponding additional losses are unavoidable because of magnetic nonlinearity of the iron core and discrete number of bars (hence a nonsinusoidal rotor) in the cage rotor.

B. Current References Optimization Beyond the TPR of ML Strategy

In ML strategy, current references for different phases have different amplitudes. As the machine torque increases, currents in phases with the largest current reference amplitudes will reach the rated value first. To extending the TPR without causing overcurrent, the ML current references needs to be reoptimized. Referring to (27) and considering the fact the current references are normalized with $\sqrt{(m/2)}I_{\alpha\beta1}$, the real amplitude of current reference in phase k, denoted by I_{k_real}, can be derived as

$$I_{k\_\mathrm{real}} = I_{\alpha\beta1}\sqrt{2\left(x_k^2 + y_k^2\right)/m}. \tag{33}$$

When I_{k_real} exceeds the rated value I_{rated}, the sine and cosine references can be decomposed into two parts, the allowable part x_{k_a}, y_{k_a} and the excessive part x_{k_e}, y_{k_e} as

$$\begin{aligned} x_{k\_a} &= \frac{I_{\mathrm{rated}}}{I_{k\_\mathrm{real}}}x_k,\ y_{k\_a} = \frac{I_{\mathrm{rated}}}{I_{k\_\mathrm{real}}}y_k \\ x_{k\_e} &= x_k - x_{k\_a},\ y_{k\_e} = y_k - y_{k\_a} \end{aligned}. \tag{34}$$

To limit I_{k_real} on the premise of circular current trajectory, x_{k_e} and y_{k_e} must be properly redistributed. Due to the property of automatically preserving the current trajectory and zero-sequence current constraints, the MLR is again utilized and an operation called MLR of excessive current references (MLRE) is derived as

$$\begin{aligned} \boldsymbol{x}_{\mathrm{MLRE}(k)} &= \boldsymbol{x}_0 + x_{k\_e\_0}\boldsymbol{R}_{\mathrm{MLR}(k)} \\ \boldsymbol{y}_{\mathrm{MLRE}(k)} &= \boldsymbol{y}_0 + y_{k\_e\_0}\boldsymbol{R}_{\mathrm{MLR}(k)} \end{aligned} \tag{35}$$

where $\boldsymbol{x}_{\mathrm{MLRE}(k)}$ and $\boldsymbol{y}_{\mathrm{MLRE}(k)}$ are the phase current references vector after MLRE(k). $x_{k\_e\_0}$ and $y_{k\_e\_0}$ are the excessive current references in phase k before the MLRE operation.

Similar with the algorithm in Fig. 2, the optimization beyond the torque range of ML strategy can be achieved by eliminating

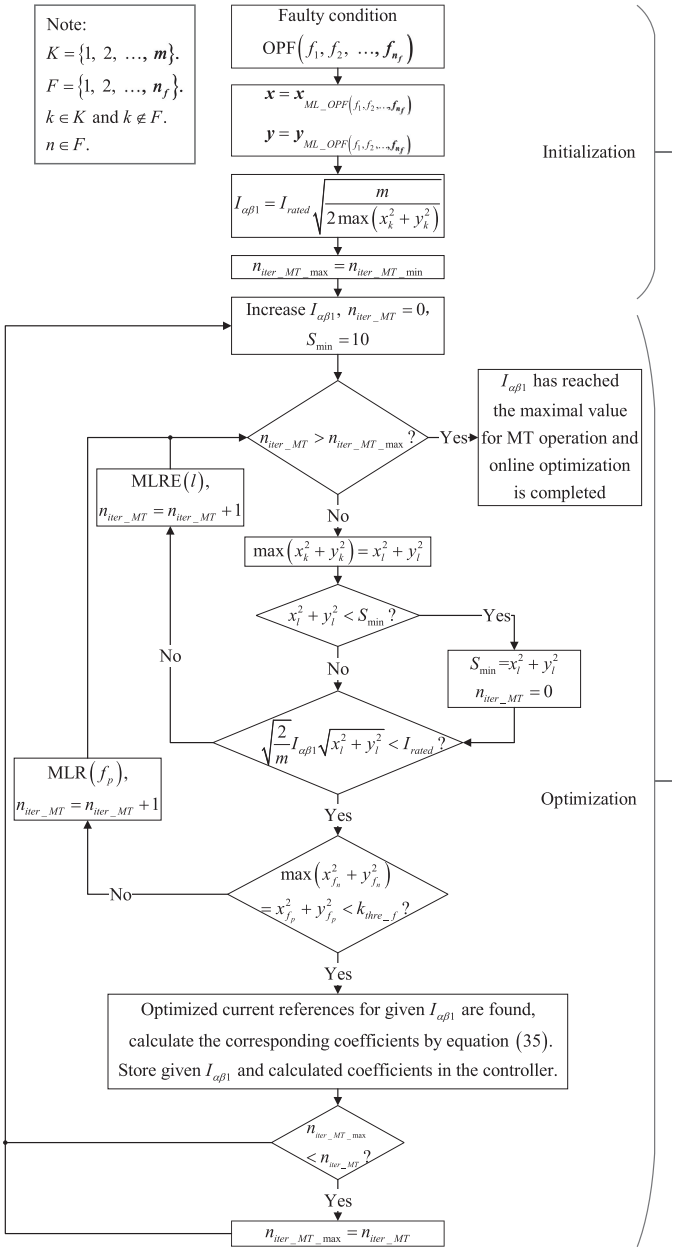

Fig. 5. Optimization algorithm for current references beyond the TPR of ML strategy.

and redistributing the references in faulty phases and the excessive current references in healthy phases at the same time. The algorithm block diagram is given in Fig. 5. The algorithm can be divided into two steps. The first step is initialization. The initial current references are set to the calculated ML references under the corresponding faulty condition and the maximal $I_{\alpha\beta 1}$ for ML strategy is calculated. The variable $n_{\mathrm{iter\_MT\_max}}$ is defined to record the maximal number of MLR and MLRE operations needed during the optimization of a given $I_{\alpha\beta 1}$. To prevent the algorithm from stopping too early, $n_{\mathrm{iter\_MT\_max}}$ is initialized with a relatively large value $n_{\mathrm{iter\_MT\_min}}$. The second step is optimization. In this step, the given $I_{\alpha\beta 1}$ is first increased by a predetermined increment, and an enumeration variable $n_{\mathrm{iter\_MT}}$ is initialized to count the number of MLR and MLRE operations. Next, the algorithm checks the terminate condition of the whole optimization procedure, whose principle will be presented later. In each round of iterations, the maximal amplitude of phase current reference is compared with the rated current first. If the amplitude is greater than the rated value, MLRE operation will be carried out to eliminate the excessive current references. This procedure is continuously performed until all amplitudes are below the rated value. As aforementioned, the MLRE will preserve the current trajectory and zero-sequence current constraints, but the constraint of the fault will be affected. Thus, current references for faulty phases are checked, furthermore eliminated with MLR if the references go beyond the threshold. When the references in healthy phases are all below the rated value and references in faulty phases are all below k_{thre_f}, the optimization for the given $I_{\alpha\beta 1}$ is completed. The coefficients needed by the current controllers are calculated as (32) and stored in controller together with $I_{\alpha\beta 1}$.

The principle of the termination check is based on a basic fact that the optimization problem will become infeasible when $I_{\alpha\beta 1}$ is above the maximal available value under MT strategy. Therefore, no matter how many MLR and MLRE operations have been done, a maximal current reference amplitude less than the rated current and small enough references in faulty phases cannot be achieved at the same time. However, the reduction of the maximal phase current reference amplitude can be an indicator of effective iterations because the final goal of the algorithm is to limit the amplitude below the rated value. Based on this principle, the algorithm checks if the maximal phase current reference amplitude cannot be further reduced even after a relatively large number of iterations. If so, the last optimization step is terminated and the last reference vector is calculated.

The optimization algorithm was evaluated on different multiphase machines under various faulty conditions, and the results are compared with ML, MT, and FRML (proposed in [22]) in Fig. 6. The optimization results from the proposed algorithm are almost the same with FRML. Minor difference is found near the maximal available $I_{\alpha\beta 1}$, which is caused by the small errors existing in the constraints.

IV. Experimental Setup and Results

A. Experimental Setup

The experiments were performed on a nine-phase IM, which can be configured in open-end configuration. In the experiments, the stator windings were connected in single-neutral-point and three-neutral-point configurations, thus, the two nine-phase SMM configurations were both evaluated. The parameters of the machine are shown in Table II. A 15-phase inverter was used and the machine is followed by a magnetic brake as the load. The system block diagram is shown in Fig. 7 and the photograph of experimental platform is shown in Fig. 8 [26].

The block diagram of the control system is shown in Fig. 9. When fault occurs, the fault locations are first detected. Fault detection is not the topic of this paper, so we use a simple method of current monitoring. When current in one phase is observed to be close to zero for a relatively long time, this phase is considered

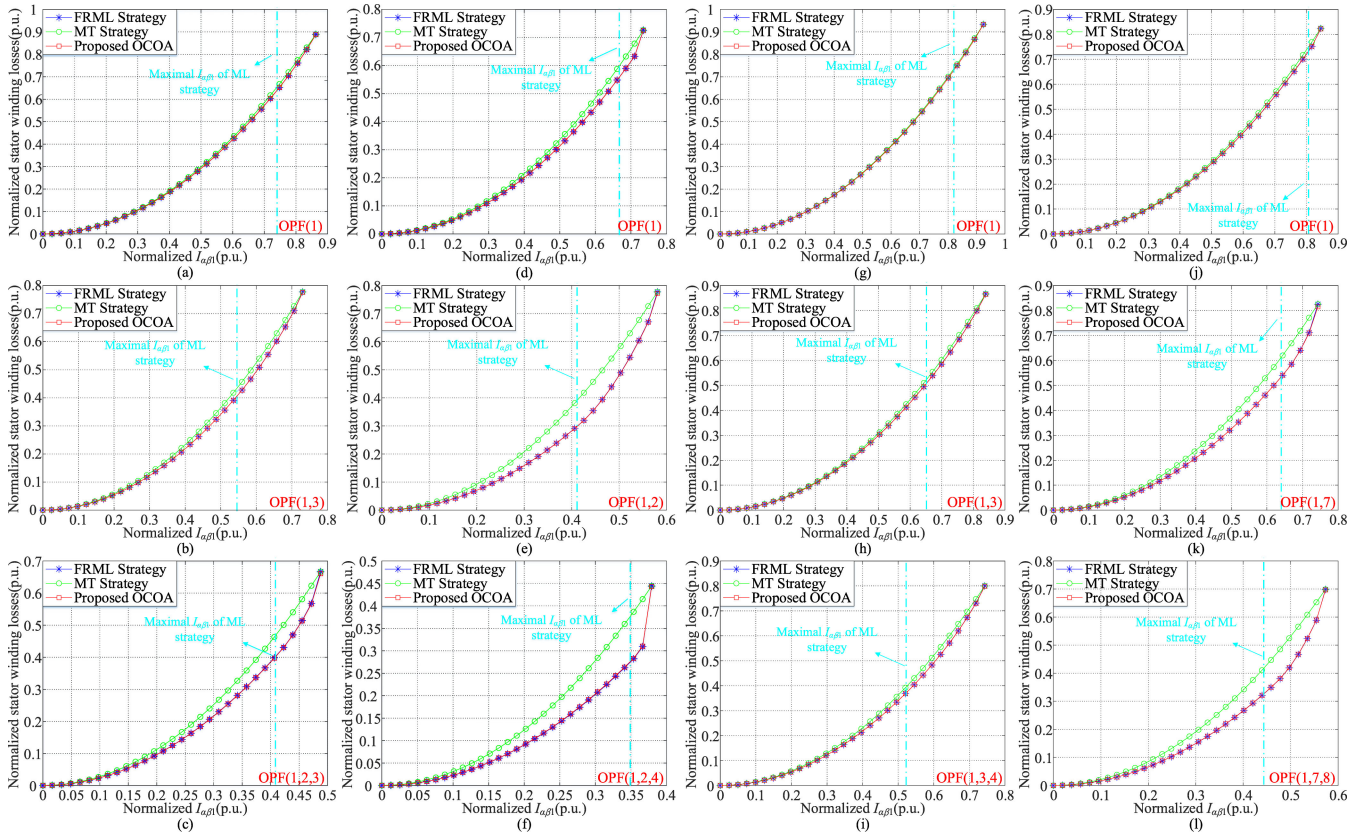

Fig. 6. Comparison of the ML, MT, FRML, and proposed OCOA in machines with different phase numbers and neutral point connections under various faulty conditions. (a)–(c) For the nine-phase machine with one neutral point. (d)–(f) For the nine-phase machine with three neutral points. (g)–(i) For the fifteen-phase machine with one neutral point. (j)–(l) For the fifteen-phase machine with five neutral points.

TABLE II
PARAMETERS OF THE NINE-PHASE IM

Machine parameter	Value	Machine parameter	Value
R_s	1.13 Ω	L_{ls}	5 mH
R_r	0.432 Ω	L_{lr}	12 mH
p	2	L_{m1}	167 mH
I_{rated}	5 A	U_{rated}	225 V

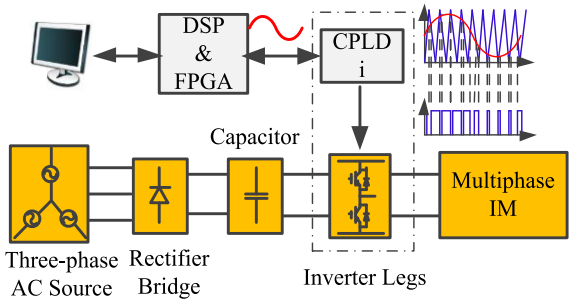

Fig. 7. Block diagram of the distributed control system.

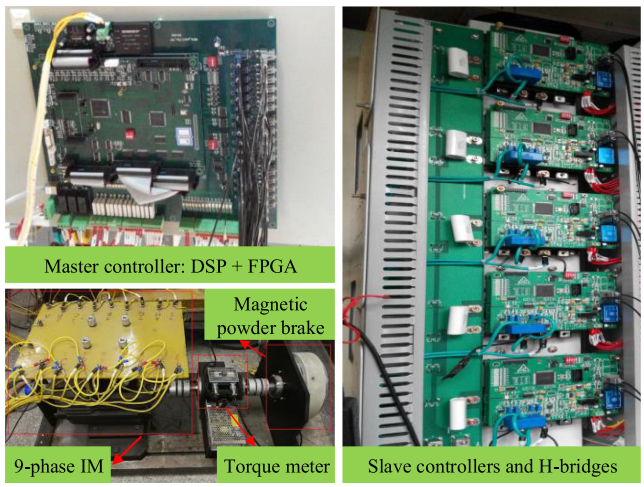

Fig. 8. Photograph of the multiphase drive system.

to be open-phase. The detected fault type is fed to the online optimization block and the coefficients are optimized and stored in the controller. The references for the current controller are calculated with these coefficients. The OCOA is carried out in each sample interval after the FOC algorithm has finished, thus has no influence on the current control. Once all the references covering the whole TPR are ready, the OCOA is terminated. If the type of the fault remains unchanged, the current references are directly calculated from the stored references. The OCOA algorithm will not be carried out until the fault type changes. Therefore, in most of the time, only the FOC algorithm runs in

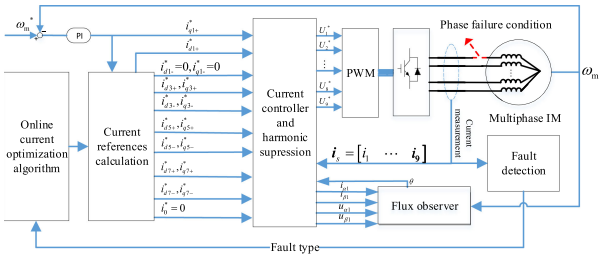

Fig. 9. Block diagram of control system.

the controller and the additional computational burden of the optimization algorithm is small.

One thing worth noticing here is that the magnetizing current reference i^*_{d1+} may need to be reduced to guarantee the maximal available torque. An optimal i^*_{d1+} can be calculated as (36). $I_{\alpha\beta1\_MT\_max}$ is the maximal available current space vector amplitude under MT strategy. If the rated value of magnetizing current is below $i^*_{d1+\_opt}$, i^*_{d1+} is set to be the rated value to avoid oversaturation of the iron core. If the rated value is larger than $i^*_{d1+\_opt}$, i^*_{d1+} is set to be $i^*_{d1+\_opt}$

$$i^*_{d1+\_\mathrm{opt}} = \frac{\sqrt{2}}{2} I_{\alpha\beta1\_\mathrm{MT\_max}}. \tag{36}$$

The optimization and control algorithm are all implemented with a TMS320F288335 DSP. The control frequency is 4 kHz and the switching frequency is 8 kHz. The dc-link voltage is 400 V and the dead-time is 5 μs. OPFs were created by disconnecting the circuit breakers between the windings of the machine and the converter. The stator phase currents were measured by a Yokogawa DL350 oscilloscope. The amplitude of the current space vector was read from the DSP.

B. Experimental Results

In the experiments, the nine-phase SMMs with a single neutral point and three neutral points were both tested. In each type of machine, three faulty conditions were considered, in which MT strategy, FRML strategy, and the proposed online method were evaluated. The current references of MT and FRML strategy were obtained via offline optimization and stored in the memory of the controller. The current references of OCOA were calculated online in the DSP. The required computation time for the optimization algorithm was recorded with the timer embedded in the DSP. The maximal available amplitude of current space vector, stator winding losses, and the fault-tolerant capability of the three strategies are compared.

The evaluated faulty conditions and corresponding computation time for the online optimization algorithm are listed in Table III. In the implementation of the algorithm, we set $k_{\mathrm{thre\_}f} = 0.0001$ and $n_{\mathrm{iter\_MT\_min}} = 50$ and the clock frequency of the TMS320F28335 was set to 150 MHz. The optimization of the ML references (the algorithm in Fig. 2) will be completed within 150 μs. Once the ML references are calculated, they will be used to regulate the currents to guarantee effective control of the post-fault currents. Later the current references will be continuously updated with the newly optimized references (obtained with the algorithm in Fig. 5) according to the value of $I_{\alpha\beta1}$. In this way, good dynamic performance and a smooth transition can be achieved during fault transients.

The experimental results for the available amplitude of current space vector and stator winding losses are given in Fig. 10. In all the six OPFs, the three strategies have almost the same maximal available current amplitude. The FRML strategy and OCOA have almost the same winding losses, which is much smaller than the MT strategy, especially when multiple phases are open-circuit. The minor difference between FRML and OCOA mainly came from the measurement error and unavoidable computational error. In general, the proposed method achieved ML operation in full TPR without offline optimization and prestored

TABLE III
EVALUATED OPFS AND CORRESPONDING COMPUTATION TIME FOR THE ONLINE OPTIMIZATION METHOD

Machine type	OPF condition	Computation time for ML references	Computation time for all references
Nine-phase single-neutral-point SMM	OPF(1)	18.0 us	10.2 ms
	OPF(1,3)	39.9 us	12.0 ms
	OPF(1,2,3)	146 us	45.8 ms
Nine-phase three-neutral-point SMM	OPF(1)	18.6 us	33.7 ms
	OPF(1,2)	47.0 us	36.1 ms
	OPF(1,2,4)	118 us	173 ms

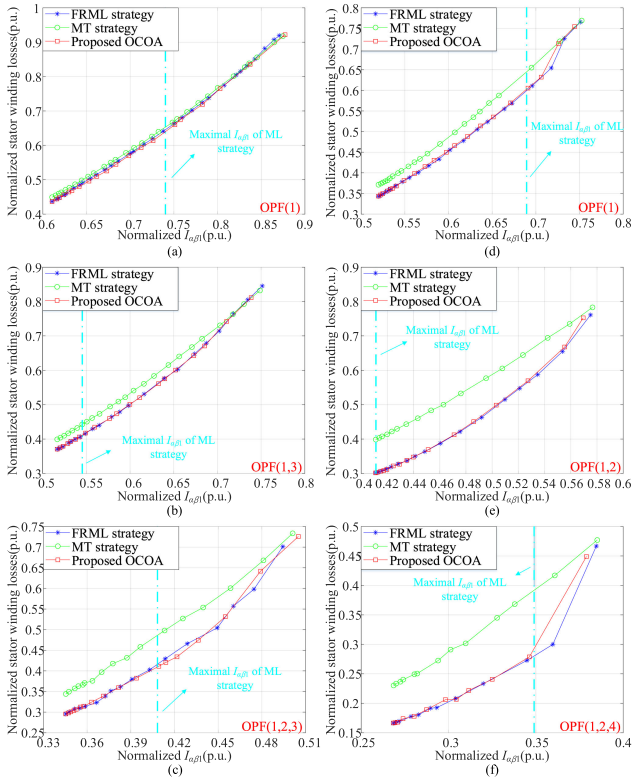

Fig. 10. Experimental comparison of the MT, FRML, and proposed OCOA. (a)–(c) For the single-neutral-point machine and (d)–(f) for the three-neutral-point machine.

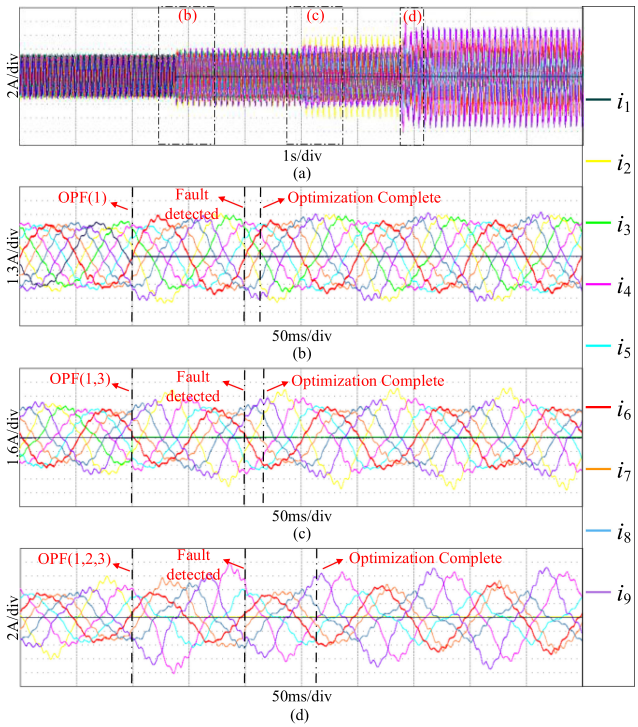

Fig. 11. Current waveforms during the fault transients of the single-neutral-point nine-phase machine. (a) Whole process. (b) From the healthy condition to the OPF(1) condition. (c) From the OPF(1) condition to the OPF(1, 3) condition. (d) From the OPF(1, 3) condition to the OPF(1, 2, 3) condition.

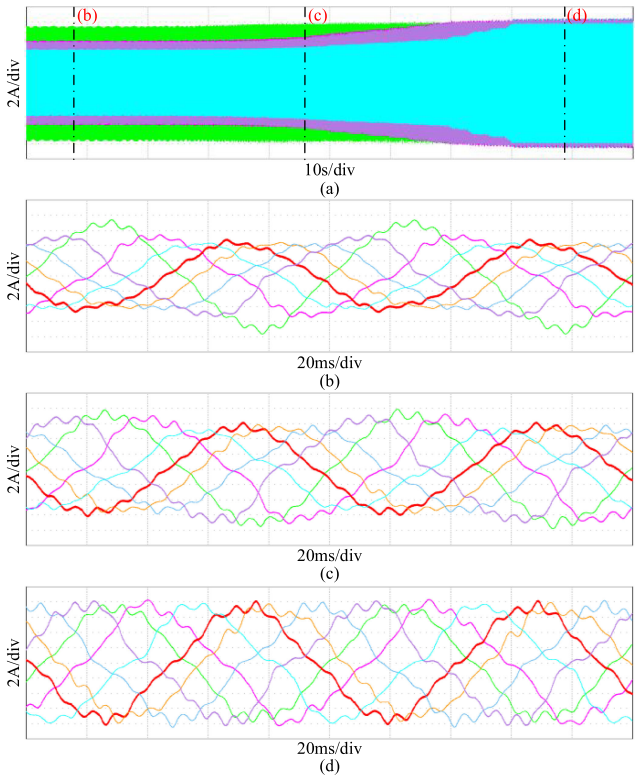

Fig. 12. Stator currents waveforms in the nine-phase SMM with a single neutral point under the OCOA strategy and OPF(1, 3) when the load was increased. (a) Whole process. (b) $I_{\alpha\beta1} \approx 0.5162$ p.u. (c) $I_{\alpha\beta1} \approx 0.6231$ p.u. (d) $I_{\alpha\beta1} \approx 0.7301$ p.u.

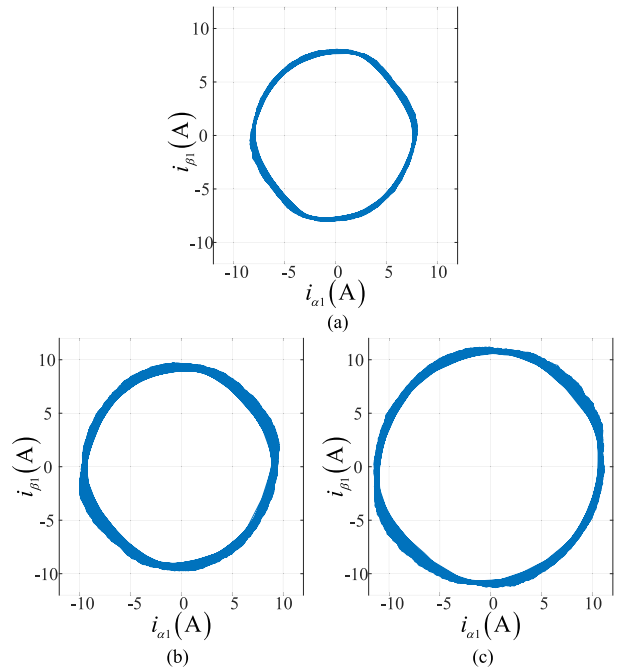

Fig. 13. Experimental results of the current space vector trajectories on $\alpha_1 - \beta_1$ plane in the nine-phase SMM with a single neutral point under the OCOA strategy and OPF(1, 3). (a) $I_{\alpha\beta1} \approx 0.5162$ p.u. (b) $I_{\alpha\beta1} \approx 0.6231$ p.u. (c) $I_{\alpha\beta1} \approx 0.7301$ p.u.

look-up tables at the cost of slightly increased computational burden of the controller.

Fig. 11 shows the current waveforms during fault transients. Fig. 11(a) shows the whole process and the three transient processes are magnified in Fig. 11(b)–(d), respectively. At the instant the fault occurred, the current in the faulty phase dropped to zero. Shortly after the fault was detected (with a latency no more than one control cycle), the ML references were calculated and used to regulate the currents. Later when new references were further optimized, the current references were adjusted based on $I_{\alpha\beta1}$ and the new references, which can be seen from the gradual variation of current amplitudes in Fig. 11 before the optimizations were completed. The transients caused by faults are smooth and swift as expected.

Fig. 12 shows the variation of current amplitudes when the load is increased. When the load torque is small, the current space vector has a small amplitude. The phase current references are the ML references, thus a relatively large difference between current amplitudes of different phases can be observed in Fig. 12(b). As the load increases, $I_{\alpha\beta1}$ exceeds the maximal available value of the ML strategy. In this region, the optimized references can achieve minimal losses and the demanded $I_{\alpha\beta1}$ without overcurrent in any phase. Therefore, amplitudes of several phases will be fixed to the rated value and the difference of phase current amplitudes are also reduced. As shown in Fig. 12(c), the current in phase 3 is fixed to the rated value and the relative difference of phase current amplitudes is narrowed compared with Fig. 12(b). When $I_{\alpha\beta1}$ reaches the maximal available value of the MT strategy, the references are

identical with the MT strategy. In the case of OPF(1, 3) and the single-neutral-point nine-phase machine, all the phases have the same current amplitude, which equals to the rated phase current as shown in Fig. 12(d).

Fig. 13 shows the current space vector trajectories in α_1-β_1 plane for the single-neutral-point machine under the OPF(1, 3) condition. The trajectories under the proposed method show a circular shape. This result shows that the proposed method has very good fault-tolerant capability. Small distortions can be observed due to the relatively concentrated winding configuration of the machine and degraded performance of harmonic suppression control. As mentioned in Section III-A, the current harmonics are larger under faulty conditions, which will cause some ripples in the torque and flux. However, the greatest ripples caused by fundamental current components have been greatly suppressed.

V. Conclusion

In this paper, an online global fault-tolerant control strategy with ML in full TPR for SMMs is proposed. This strategy is based on the proposed OCOA, which can be adopted to any SMMs under any OPFs. The proposed method allows us to compute the current references with the minimal stator winding losses in the whole TPR under various OPFs in real-time. Compared to the offline method, the proposed scheme achieves the same stator winding losses reduction and fault-tolerant capability without offline optimizations and prestored look-up tables. Due to its generality and extensibility, the proposed method can be combined with modular multiphase converters to form a universal fault-tolerant multiphase converter system that can adapt to the varied machine phase numbers in different drives and applications. Additionally, the advantage of avoiding offline optimization and storage of look-up tables becomes more significant for machines with high phase numbers, where the number of possible OPFs can be extremely large. The proposed strategy has been validated by experimental results on nine-phase SMMs with two different types of neutral point connections.

References

[1] E. Levi, R. Bojoi, F. Profumo, H. A. Toliyat, and S. Williamson, "Multiphase induction motor drives—A technology status review," *IET Electr. Power Appl.*, vol. 1, no. 4, pp. 489–516, 2007.

[2] E. Levi, "Multiphase electric machines for variable-speed applications," *IEEE Trans. Ind. Electron.*, vol. 55, no. 5, pp. 1893–1909, May 2008.

[3] E. Levi, "Advances in converter control and innovative exploitation of additional degrees of freedom for multiphase machines," *IEEE Trans. Ind. Electron.*, vol. 63, no. 1, pp. 433–448, Jan. 2016.

[4] E. Levi, F. Barrero, and M. J. Duran, "Multiphase machines and drives - Revisited," *IEEE Trans. Ind. Electron.*, vol. 63, no. 1, pp. 429–432, Jan. 2016.

[5] M. A. Elgenedy, A. A. Elserougi, A. S. Abdel-Khalik, A. M. Massoud, and S. Ahmed, "A space vector PWM scheme for five-phase current-source converters," *IEEE Trans. Ind. Electron.*, vol. 63, no. 1, pp. 562–573, Jan. 2016.

[6] L. Zarri *et al.*, "Detection and localization of stator resistance dissymmetry based on multiple reference frame controllers in multiphase induction motor drives," *IEEE Trans. Ind. Electron.*, vol. 60, no. 8, pp. 3506–3518, Aug. 2013.

[7] N. K. Nguyen, F. Meinguet, E. Semail, and X. Kestelyn, "Fault-tolerant operation of an open-end winding five-phase PMSM drive with short-circuit inverter fault," *IEEE Trans. Ind. Electron.*, vol. 63, no. 1, pp. 595–605, Jan. 2016.

[8] M. J. Duran and F. Barrero, "Recent advances in the design, modeling, and control of multiphase machines—Part II," *IEEE Trans. Ind. Electron.*, vol. 63, no. 1, pp. 459–468, Jan. 2016.

[9] A. Mohammadpour and L. Parsa, "Global fault-tolerant control technique for multiphase permanent-magnet machines," *IEEE Trans. Ind. Appl.*, vol. 51, no. 1, pp. 178–186, Jan./Feb. 2015.

[10] H. S. Che, E. Levi, M. Jones, M. J. Duran, W. Hew, and N. A. Rahim, "Operation of a six-phase induction machine using series-connected machine-side converters," *IEEE Trans. Ind. Electron.*, vol. 61, no. 1, pp. 164–176, Jan. 2014.

[11] F. Betin and G. Capolino, "Shaft positioning for six-phase induction machines with open phases using variable structure control," *IEEE Trans. Ind. Electron.*, vol. 59, no. 6, pp. 2612–2620, Jun. 2012.

[12] Y. Zhao and T. A. Lipo, "Modeling and control of a multi-phase induction machine with structural unbalance," *IEEE Trans. Energy Convers.*, vol. 11, no. 3, pp. 578–584, Sep. 1996.

[13] Y. Zhao and T. A. Lipo, "Space vector PWM control of dual three phase induction machine using vector space decomposition," in *Proc. IEEE Ind. Appl. Soc. Annu. Meet.*, 1994, vol. 1, pp. 742–749.

[14] R. Kianinezhad, B. Nahid-Mobarakeh, L. Baghli, F. Betin, and G. Capolino, "Modeling and control of six-phase symmetrical induction machine under fault condition due to open phases," *IEEE Trans. Ind. Electron.*, vol. 55, no. 5, pp. 1966–1977, May 2008.

[15] A. Pantea *et al.*, "Six-phase induction machine model for electrical fault simulation using the circuit-oriented method," *IEEE Trans. Ind. Electron.*, vol. 63, no. 1, pp. 494–503, Jan. 2016.

[16] Z. Liu, Z. Zheng, and Y. Li, "Enhancing fault-tolerant ability of a nine-phase induction motor drive system using fuzzy logic current controllers," *IEEE Trans. Energy Convers.*, vol. 32, no. 2, pp. 759–769, Jun. 2017.

[17] F. Lin, Y. Hung, and M. Tsai, "Fault-tolerant control for six-phase PMSM drive system via intelligent complementary sliding-mode control using TSKFNN-AMF," *IEEE Trans. Ind. Electron.*, vol. 60, no. 12, pp. 5747–5762, Dec. 2013.

[18] H. S. Che, M. J. Duran, E. Levi, M. Jones, W. Hew, and N. A. Rahim, "Postfault operation of an asymmetrical six-phase induction machine with single and two isolated neutral points," *IEEE Trans. Power Electron.*, vol. 29, no. 10, pp. 5406–5416, Oct. 2014.

[19] J.-R. Fu and T. A. Lipo, "Disturbance-free operation of a multiphase current-regulated motor drive with an opened phase," *IEEE Trans. Ind. Appl.*, vol. 30, no. 5, pp. 1267–1274, Sep./Oct. 1994.

[20] S. Dwari and L. Parsa, "An optimal control technique for multiphase PM machines under open-circuit faults," *IEEE Trans. Ind. Electron.*, vol. 55, no. 5, pp. 1988–1995, May 2008.

[21] A. Mohammadpour and L. Parsa, "A unified fault-tolerant current control approach for five-phase PM motors with trapezoidal back EMF under different stator winding connections," *IEEE Trans. Power Electron.*, vol. 28, no. 7, pp. 3517–3527, Jul. 2013.

[22] F. Baneira, J. Doval-Gandoy, A. G. Yepes, Ó. López, and D. Pérez-Estévez, "Control strategy for multiphase drives with minimum losses in the full torque operation range under single open-phase fault," *IEEE Trans. Power Electron.*, vol. 32, no. 8, pp. 6275–6285, Aug. 2017.

[23] E. Levi, "FOC: field-oriented control," in *Power Electronics and Motor Drives*. Amsterdam, The Netherlands: Elsevier, 2016, pp. 24.1–24.31.

[24] Z. Liu, Z. Zheng, L. Xu, K. Wang, and Y. Li, "Current balance control for symmetrical multiphase inverters," *IEEE Trans. Power Electron.*, vol. 31, no. 6, pp. 4005–4012, Jun. 2016.

[25] A. G. Yepes, J. Malvar, A. Vidal, O. López, and J. Doval-Gandoy, "Current harmonics compensation based on multiresonant control in synchronous frames for symmetrical n-phase machines," *IEEE Trans. Ind. Electron.*, vol. 62, no. 5, pp. 2708–2720, May 2015.

[26] Z. Liu, Z. Zheng, S. D. Sudhoff, C. Gu, and Y. Li, "Reduction of common-mode voltage in multiphase two-level inverters using SPWM with phase-shifted carriers," *IEEE Trans. Power Electron.*, vol. 31, no. 9. pp. 6631–6645, Sep. 2016.

Jiawei Sun (S'17) was born in Ningxia, China, in 1994. He received the B.S. degree in electrical engineering from Tsinghua University, Beijing, China, in 2017, where he is currently working toward Ph.D. degree in power electronics and electrical drives at the State Key Laboratory of Power System, Department of Electrical Engineering.

His current research interests include position sensor-less control of ac motors and multiphase machine drives.

Zicheng Liu (M'18) was born in Shandong, China, in 1989. He received the B.S. degree in hydropower engineering from Huazhong University of Science and Technology (HUST), Wuhan, China, in 2011, and the Ph.D. degree in electrical engineering from Tsinghua University, Beijing, China, in 2016.

During Otcober 2014 to March 2015, he was a Visiting Student with Purdue University, West Lafayette, IN, USA. During June 2016 to September 2018, he was a Postdoc Researcher with Beijing Jiaotong University, Beijing. He is currently an Associate Professor with HUST. His research interests include multiphase motor control systems and transportation electrification.

Zedong Zheng (M'09–SM'19) was born in Shandong, China, in 1980. He received the B.S. and Ph.D. degrees in electrical engineering from Tsinghua University, Beijing, China, in 2003 and 2008, respectively.

He is currently an Associate Professor with the Department of Electrical Engineering, Tsinghua University. His current research interests include power electronics converters and high-performance motor control systems.

Yongdong Li (M'08) was born in Hebei, China, in 1962. He received the B.S. degree from Harbin Institute of Technology, Harbin, China, in 1982, and the M.S. and Ph.D. degrees from Institut National Polytechnique de Toulouse, Toulouse, France, in 1984 and 1987, respectively.

Since 1996, he has been a Professor with the Department of Electrical Engineering, Tsinghua University, Beijing, China. He was also an Invited Professor with the Institut National Polytechnique de Toulouse. From 2011 to 2014, he was the Dean of the School of Electrical Engineering, Xinjiang University, Urumqi, China. His current research interests include power electronics, machine control, and wind power generation.

Prof. Li is also a Senior Member of the China Electro-Technique Society, the Vice Chairman of the China Power Electronics Society, and the Vice Chairman of the Electrical Automation Committee of China Automation Association.